Published in final edited form as:
*J Mol Cell Cardiol*. 2010 January ; 48(1): 112. doi:10.1016/j.yjmcc.2009.09.019.

# A Novel Computational Model of the Human Ventricular Action Potential and Ca Transient

**Eleonora Grandi**[1], **Francesco S. Pasqualini**[2], and **Donald M. Bers**[1]

[1]Department of Pharmacology, University of California, Davis, USA

[2]Department of Physics and Material Engineering, Technical University of Marche, Ancona, Italy

## Abstract

We have developed a detailed mathematical model for Ca handling and ionic currents in the human ventricular myocyte. Our aims were to: 1) simulate basic excitation-contraction coupling phenomena; 2) use realistic repolarizing K current densities; 3) reach steady-state. The model relies on the framework of the rabbit myocyte model previously developed by our group, with subsarcolemmal and junctional compartments where ion channels sense higher [Ca] vs. bulk cytosol. Ion channels and transporters have been modeled on the basis of the most recent experimental data from human ventricular myocytes. Rapidly and slowly inactivating components of $I_{to}$ have been formulated to differentiate between endocardial and epicardial myocytes. Transmural gradients of Ca handling proteins and Na pump were also simulated. The model has been validated against a wide set of experimental data including action potential duration (APD) adaptation and restitution, frequency-dependent increase in Ca transient peak and $[Na]_i$. Interestingly, Na accumulation at fast heart rate is a major determinant of APD shortening, *via* outward shifts in Na pump and Na-Ca exchange currents. We investigated the effects of blocking K currents on APD and repolarization reserve: $I_{Ks}$ block does not affect the former and slightly reduces the latter; $I_{K1}$ blockade modestly increases APD and more strongly reduces repolarization reserve; $I_{Kr}$ blockers significantly prolong APD, an effect exacerbated as pacing frequency is decreased, in good agreement with experimental results in human myocytes. We conclude that this model provides a useful framework to explore excitation-contraction coupling mechanisms and repolarization abnormalities at the single myocyte level.

### Keywords

Human ventricular myocyte; computer model; K current block; reverse rate-dependence

## Introduction

In the past years, mathematical modeling has become an important tool in understanding cardiac electrophysiology and its derangements (e.g. arrhythmias). Models of excitation-contraction coupling (ECC) in several species have been developed (such as guinea pig [1], rabbit [2], mouse [3] and canine [4]) and proven useful to study the mechanisms underlying disturbances of cardiac electrophysiology due to various conditions [5] or the effects of drugs

Correspondence: Donald M Bers, Ph.D., Department of Pharmacology, University of California, Davis, 451 Health Sciences Drive, GBSF Room 3513, Davis, CA 95616-8636, Phone: (530) 752-6517, Fax: (530) 752-7710, dmbers@ucdavis.edu.

[6]. Although these animal models are commonly used to study cellular cardiac electrophysiology in a range of disease states, animal and human cardiomyocytes differ in important aspects that may influence the arrhythmogenic mechanisms, such as action potential (AP) shape, duration (APD) and restitution, range of normal heart rates, and relative contribution of ionic currents (where density and kinetics vary among species) to AP repolarization. There are recent mathematical models of electrical and ionic homeostasis in human ventricular myocytes [7-11]. Among these, the Panfilov group has comprehensively modeled the individual currents generating an AP, with APD and conduction velocity restitution properties in agreement with experimental measurements *(TNNP04 and TP06)* [8, 10]. Reduced versions of these models were also implemented for large-scale spatial simulations [9,12]. Another relevant model for human ventricular myocytes was published in 2004 by Iyer et al. *(IMW)* [11]. This model addresses whole-cell Ca homeostasis carefully and accurately reproduces diverse aspects of ECC. The most relevant ionic currents are formulated with Markovian chains, which make this model much more complex than those previously described.

Each of the existing models has particular strengths (and weaknesses) and may be more suited for certain investigations; however, some issues unresolved in current models are: 1) the quantitative importance of individual K currents for AP repolarization; 2) the rate-dependence of AP prolongation upon K channel block, and 3) the cause of APD shortening at faster heart rates. Thus, use of these models to predict alterations of AP repolarization due to drugs or diseases should be made with caution. In addition, since the introduction of many of these models in their original form, new information regarding human myocytes electrophysiology has become available. For example, the increase in [Ca] upon Ca-induced Ca release appears to be higher just under the sarcolemma than in bulk cytosol, and this higher [Ca] is detected by Na-Ca exchanger (NCX) [13]. Here we have taken advantage of the rabbit ECC model developed by Shannon et al. [2], which includes this additional subsarcolemmal compartment (SL) and provides a detailed description of Ca handling. We also provide updated ionic currents densities and kinetics based on the most recent experimental measurements in human myocytes.

The resulting model is stable and capable of reproducing diverse behaviors measured experimentally in isolated human ventricular myocytes including: 1) AP shape of epicardial and endocardial cells; 2) Ca transient morphology and kinetics; 3) rate-dependent changes of APD, Ca transient and $[Na]_i$; 4) APD restitution; 5) effect of blocking K currents on APD.

## Methods

### Model development

The ventricular AP model relies on the framework of the rabbit myocyte model developed by Shannon et al. [2] including both a cleft space (between sarcoplasmic reticulum (SR) and sarcolemmal membrane) where Ca induced Ca release occurs, and a separate SL compartment, which is a narrow space just under the rest of the cell membrane. The human myocyte model consists of a system of 38 ordinary differential equations describing the rate of change of membrane potential, gating variables describing the kinetics of ion channels, intracellular concentrations of Na and Ca ions, and the dynamics of intracellular Ca cycling processes. Model equations and parameters are given in the Online Appendix. Fitting of fast sodium and L-type calcium currents is shown in supplementary Figures S1 and S2. Here, a brief description of K current fitting is provided. The Na-Ca exchanger was formulated as described in [13] and implemented in Shannon et al. [2], as well as Na pump, Ca-activated Cl, background Na, Ca, K and Cl currents.

### Slowly activating delayed rectifier K current $I_{Ks}$

$I_{Ks}$ has been modeled to fit steady-state activation (Figure 1A), tail current magnitudes (Figure 1C), time constants of activation (Figure 1B and D) and deactivation (Figure 1B) obtained at physiological temperature by Virág et al. [14]. $I_{Ks}$ conductance was set to 0.0035 mS/μF to match tail current magnitudes measured in human ventricle (Figure 1C).

### Rapidly activating delayed rectifier K current $I_{Kr}$

$I_{Kr}$ steady-state curves (not shown) reflect experimental data from Zhou et al. [15] (activation) and Johnson et al. [16] (inactivation). Time constants of activation and deactivation are derived from experiments performed by Jost et al. [17,18] at 37°C (Figure 2A). $I_{Kr}$ conductance was set to 0.035 mS/μF to match tail current recordings in human ventricular myocytes [19] (Figure 2B). Simulated $I_{Kr}$ during an envelope of tails protocol is depicted in Figure 2C.

### Inward rectifier K current $I_{K1}$

Figure 2D shows the good agreement of our $I_{K1}$ model with experimental current-voltage curves obtained by Magyar et al. [20] and Jost et al. [17, 18] at physiological temperature.

### Transient outward K current $I_{to}$

Two components of $I_{to}$ are found in the human ventricle: $I_{to,fast}$ exhibiting fast recovery from inactivation and $I_{to,slow}$ exhibiting relatively slow kinetics of recovery from inactivation. Slow and fast components were formulated based on the steady-state data (Figure 3A, B and F) from Näbauer et al. [21] and the kinetic data obtained at 37°C by Näbauer et al. [21], Wettwer et al. [22] and Varró et al. [23] (Figure 3C-E and G). In epicardial myocytes the fast component is dominant, whereas endocardial cells lack appreciable $I_{to,fast}$ [21]. Accordingly, in our epicardial digital cell, $I_{to,fast}$ comprises 88% of total $I_{to}$, whereas in endocardial cells the slowly recovering component accounts for most of $I_{to}$ (96.4%). Figure 3G shows the agreement between the simulated and experimental (Varró et al. [23] and Näbauer et al. [21]) $I_{to}$ recovery from inactivation in human epicardial and endocardial myocytes. Total $I_{to}$ conductance was set to 0.13 mS/μF in epicardium and 0.04 mS/μF in endocaridum to match the experimental current-voltage relationship from Varró et al. [23] and Näbauer et al. [21] (Figure 3F). There may be additional epi- endocardial difference in ion channel/transporters that could be included, but our baseline model does not incorporate these (see online supplement).

### Numerical implementation and simulations

Model differential equations were implemented in Matlab (Mathworks Inc., Natick, MA, U.S.A.) and solved numerically using a variable order solver (ode15s) [24]. APD was measured as the interval between AP upstroke and 90% repolarization level ($APD_{90}$). APD restitution was assessed with a dynamic protocol: after establishing a steady-state at a basic cycle length of 600 ms, extrastimuli were applied at 20 cycle intervals, reducing the coupling interval in decrements of 40, 20 and 10 ms from the drive cycle length. Stimuli were also delivered at coupling intervals larger than the steady-state drive cycle length as in Morgan et al. [25].

## Results

### AP and Ca transient characteristics

In Figure 4A a steady-state epicardial AP simulated at 1 Hz pacing rate is depicted. The AP shows the characteristic spike notch dome morphology found for epicardial cells. APD is 283 ms, resting potential is −81.3 mV, maximum plateau potential is 25 mV, all in agreement with experimental data [26-28]. Model AP amplitude is 124 mV, which is in the midrange of experimental measurements (100 mV [29], 132 mV [27], and 135 mV [21]). Model maximal upstroke velocity is 372 V/s (experimental measurements range from 228±20 V/s [26] to 446

±46 V/s [30]). The rise in free junctional cleft [Ca] (Figure 4C) resulting from L-type Ca current (Figure 4F) initiates Ca-induced Ca release from the SR (total Ca load ~95 μmol/L cytosol). Calcium in the cleft peaks very rapidly at a high value before diffusing through the SL to the cytosol. Also the SL Ca transient (Figure 4D) rises higher than the cytosolic [Ca] (as estimated by Weber et al. [31]) and decreases as Ca diffuses into the bulk cytosol. The cytosolic [Ca] (Figure 4B) rises from a diastolic level of 89 nM to a peak value of 0.4 μM and declines with a time constant of 175 ms, comparable to values experimentally obtained by Piacentino at el. [28] at 37°C. Figure 4 also shows the major ionic currents generating and shaping the AP, which agree in amplitude and time course with those measured experimentally.

## Response to frequency

Steady-state APs last 364 and 385 ms at 0.25 Hz in epicardial and endocardial cells respectively. $APD_{90}$ decreases to 219 and 236 ms as the pacing rate is increased to 3 Hz (Figure 5A). The predicted APD shortening is in the range of experimental variability (Figure 5B), as is the duration of the AP [27, 29, 32, 33]. The APD restitution curve for a single endocardial cell is shown in Figure 5C (*dashed line*) and approximates the experimental curve (*circles*) found by Morgan et al. [25] with a similar protocol (see Methods).

Figure 6A shows the change in cytosolic calcium transient peak when increasing the pacing frequency in a stepwise fashion between 0.25 and 3 Hz. In our epicardial and endocardial cell models (*solid* and *dashed lines*) cytosolic [Ca] peaks at ~250 nM at the slowest rate and increases substantially as the pacing frequency increases. Model predictions are in agreement with [Ca] measurements (aequorin light emission) in ventricular muscle strips [32] and isolated trabeculae [34]. In Figure 6B the corresponding percentage increase in $[Na]_i$ with increasing frequency is shown (being $[Na]_i$~7.25 mM at 0.25 Hz). The relative changes in $[Na]_i$ are similar to those measured in human myocardium [35], although a possible overestimation of absolute $[Na]_i$ was acknowledged [35].

A somewhat surprising emergent property was that $[Na]_i$ accumulation contributes significantly to $APD_{90}$ shortening at faster pacing rates. In fact, changes in $I_{NaK}$ (from 0.2 to 0.3 to 0.4 A/F) are the most significant increase in outward current during the initial phase of the AP plateau when increasing the pacing rate from 0.25 to 1 Hz to 2 Hz (Figure S3, A). In addition, the increased $[Na]_i$ causes Na-Ca exchange current to shift in the outward direction (Figure S3, B), thus contributing to APD shortening. We have tested this further by pacing the epicardial cell at high frequency (2 Hz), but setting $[Na]_i$ to the steady-state level predicted at 0.5 Hz ($[Na]_i$=7.65 mM, Figure 5A, ○). Under these conditions, APD does not adapt to frequency and lasts ~330 ms (as when pacing at 0.5 Hz). When the cell is stimulated at 0.5 Hz but $[Na]_i$ is set to the steady-state level predicted at 2-Hz stimulation (9.1 mM), APD is short (~240 ms), just like when the cell is paced at 2 Hz (Figure 5A, ●). Furthermore, if the increased $[Na]_i$ is only sensed by $I_{NaK}$, APD is decreased from 330 to 265 ms, but if only sensed by $I_{NaCa}$, APD shortens to only 283 ms. If both sense the increased $[Na]_i$ then APD shortens to 240 ms. This indicates that $I_{NaK}$ is dominant ~2:1 over $I_{NaCa}$ in this effect. Moreover, our results suggest that fast $I_{Na}$ and background Na current do not contribute to APD adaptation *per se*, but do contribute to Na accumulation at fast pacing rates (not shown). In Figure 6C we show the changes in $APD_{90}$ predicted by our epicardial cell model at 1 Hz when clamping $[Na]_i$ at various levels. Simulation of partial Na pump blockade (50%) shows a biphasic impact on APD: repolarization prolongs instantaneously (due to the reduction in an outward current), and then shortens as Na starts accumulating intracellularly reaching a new shorter steady APD (Figure 6D).

### Effect of K current block

Next we assessed the contribution of $I_{Ks}$ and $I_{Kr}$ to ventricular repolarization by analyzing the effect of their complete block on APD. The model predicts no changes in AP duration or morphology when $I_{Ks}$ is silenced (Figure 7B, ▲ vs. ●), in agreement with experimental results in isolated ventricular myocytes ([18, 36], Figure 7A). This does not mean that $I_{Ks}$ is irrelevant, but is consistent with the idea that in normal human ventricle it is only functionally important upon β-adrenergic stimulation to decrease APD in the fight or flight response.

On the other hand, $I_{Kr}$ blockade significantly prolongs APD in human ventricular myocytes (Figure 7A [36]) and in our model (Figure 7B, ◆ vs. ●). Furthermore, $I_{Kr}$ block-induced AP prolongation is more prominent in our endocardial myocyte model, and both cell types show reverse frequency-dependence, i.e. block-induced prolongation was more pronounced at lower pacing frequencies (Figure 7D, *solid* and *dashed lines*), as measured in canine cardiac muscle preparations and human ventricular myocytes (Figure 7, C and D, *symbols*) [36, 37].

It now seems established that $I_{Ks}$ block in absence of sympathetic stimulation plays little role in increasing normal human (and large mammal) ventricular APD. However, when the repolarization reserve is attenuated (e.g., by drugs or diseases that reduce other repolarizing currents), $I_{Ks}$ may become increasingly important in limiting AP prolongation [36]. Our simulations predict that $I_{Kr}$ block increases APD by 27% when $I_{Ks}$ is present (Figure 7B, ◆ vs. ●), vs. 33% with $I_{Ks}$ block (Figure 7B, ■ vs. ▲), that is an increase of 22% attributable to the loss of $I_{Ks}$ contribution to repolarization reserve. A more modest increase (16%) was observed in the experimental work of Jost et al. [18] (Figure 7A), with a greater APD prolongation upon $I_{Kr}$ block (~56%).

Silva and Rudy [38] have identified a Markov model of $I_{Ks}$ from human data. Used in their guinea pig AP model, this $I_{Ks}$ formulation generated AP shortening at fast rates, but a very large maximal conductance was required for normal AP repolarization. We have used their formulation of human $I_{Ks}$ in our AP model (with a moderate maximal conductance of 0.0065 mS/μF, Ca-independent). Figure S4, A *shows* $I_{Ks}$ traces when pacing the digital cell at 1 and 3 Hz. At fast rate we observe an increase in open-state accumulation, responsible for the initial current increase, and closed-state accumulation in states that activate rapidly, creating a reserve that allows an increase in the peak current [39]. However, this increase has negligible effects on APD adaptation, which is entirely due to increase in $[Na]_i$ (e.g., no adaptation occurs when [Na] is clamped at low values, as already discussed). When $I_{Kr}$ is blocked, $I_{Ks}$ increase is slightly enhanced at high frequencies (Figure S4, B), but shortening is hardly affected (26% vs. 22% APD shortening when going from 1 to 3 Hz pacing rate), and the reverse rate-dependence is similar to that obtained with our $I_{Ks}$ model (not shown).

When blocking $I_{K1}$ (50% to reproduce experimental block with 10 μM $BaCl_2$), APD is moderately increased as observed experimentally (Figure 8, ▲ vs. ●), and the extent of AP prolongation (~10% vs. 5% in experiments) is independent of the pacing rate. $I_{Kr}$ block increases APD by 27% when $I_{K1}$ is present (Figure 8B, ◆ vs. ●), vs. 35% in presence of $I_{K1}$ block (Figure 8B, ■ vs. ▲), suggesting a 30% increase in $I_{Kr}$ blocking effect when $I_{K1}$ is partially inhibited, similar to that observed experimentally by Jost et al. [18] (~34%, Figure 8A).

### Epicardial vs. endocardial cells

Changes in $I_{to}$ current densities and ratios between $I_{to,fast}$ and $I_{to,slow}$ (as measured by Näbauer et al. [21]) allowed differentiating endocardial and epicardial myocyte models. No difference has been reported in $I_{Ks}$ density between the two cell types [30]. In epicardial myocytes, $I_{to}$ has larger conductance and recovers more rapidly from inactivation. This confers the typical

AP shape, with a pronounced notch in the early repolarization phase (Figure 4A). In endocardial myocytes, the smaller $I_{to}$ leads to absence of AP notch (Figure 7B), longer APD (296 ms vs. 283 ms at 1 Hz pacing rate, Figure 5A) and higher sensitivity to $I_{Kr}$ block (Figure 7D). APD adaptation does not differ between epicardial and endocardial digital cells (Figure 5A), as also reported experimentally [26,27].

Transmural heterogeneity in Ca handling proteins has been described in canine ventricular myocytes. Xiong et al. [40] reported a greater NCX current and mRNA and protein levels, and Laurita et al. [41] reported significantly more SR Ca-ATPase (SERCA) expression and function in epicardial vs. endocardial myocytes. In failing human ventricle, Prestle et al. [42] showed lower SERCA2 and phospholamban protein levels in endocardium vs. epicardium, but similar NCX mRNA levels. In nonfailing hearts there was only a trend (non-significant) toward lower SERCA2a and phospholamban in endo- vs. epicardium and no NCX mRNA difference [42]. To explore the impact of these possible changes, we simulated increases of SERCA and NCX by 20 and 10% at the epicardium and reducing by the same percent at the endocardium (i.e. gradients of ~40% and 20% for SERCA and NCX). This resulted in slightly larger Ca transient amplitude, delayed time to peak and rate of $[Ca]_i$ decline in endocardium (Figure S5). The slowed Ca transient decay was also reported in dog heart transmural wedges [41]. Frequency-dependent changes in APD, Ca transient amplitude and $[Na]_i$ are only slightly altered in both cell types (Figure S6 vs. Figures 5A-B and 6A-B), but none of our conclusions are altered (e.g. the $[Na]_i$ effect on APD adaptation).

In canine myocardium, $I_{NaK}$ decreases from epicardium to endocardium [43]. Further incorporating a Na pump transmural gradient (+/-20% in epicardium/endocardium), causes a consequent transmural $[Na]_i$ gradient, but the fractional increase in Ca and Na and decrease of APD with frequency were not appreciably altered vs. Figure S6B-D (not shown). However, APD in endocardial cells became shorter than in epicardial cells (277 vs. 296 ms at 1 Hz) due to greater $[Na]_i$(8.8 vs. 7.8 mM at 1 Hz).

## Discussion

Here we propose an improved computational model of the human epicardial and endocardial myocytes, based on some of the best features from different prior models combined with newer data. We have validated the model against experimental results not included in the fitting process. The model predicts experimental properties characteristic of human myocytes, including: 1) APD shortening as a function of pacing frequency (adaptation); 2) Ca transient morphology and kinetics; 3), monotonic increase of the intracellular Ca transient peak as a function of pacing frequency; 4) monotonic increase of $[Na]_i$ as a function of pacing frequency; 5) effects of $I_{Ks}$, $I_{Kr}$, and $I_{K1}$ blockade on APD and its rate-dependence.

### Responses to frequency

Model results suggest that increase of intracellular [Na] at fast rates is the major mechanism responsible for APD adaptation. When accumulation of $[Na]_i$ at high frequencies was prevented by clamping $[Na]_i$ at the constant level predicted at slow rates, APD shortening did not occur and APD was comparable to that obtained at low frequency. Thus, changes in $I_{NaK}$ and $I_{NaCa}$ produced by changes in $[Na]_i$ at different pacing frequencies have significant effects on $APD_{90}$. In fact, experiments in failing human myocytes have shown that $[Na]_i$ can influence APD [44]. Our model predictions reveal a potential direct role for $[Na]_i$ (other than its involvement in the regulation of $[Ca]_i$ *via* Na-Ca exchanger) that could be tested experimentally. Indeed, a biphasic effect of $I_{NaK}$ inhibition on APD (as in Figure 6D) has been reported in guinea pig ventricular myocytes [45] and human atrial fibers [46]. Our model suggests that gradual AP shortening following instantaneous prolongation is due to Na accumulation over several beats. We also speculate that the increased $[Na]_i$ in heart failure may

limit AP prolongation caused by reduced K channel conductance and increased late Na current. An effect of $[Na]_i$ accumulation to shorten APD has been shown previously in guinea pig (but considered more modest) [1] and human [11] models.

Our model provides an accurate description of Ca handling in the human ventricular myocyte. Experimentally, in nonfailing human myocardium, $[Ca]_i$ and twitch force increase monotonically with frequency over a wide range of pacing rates (from 0.25 to 3 Hz) [32]. This behavior is predicted by our model and IMW, whereas in TP06 the Ca transient peak increases by 2, 7 and 12 fold when pacing frequency is increased from 0.25 to 0.5, 1 and 2 Hz respectively (e.g., much more than experimentally observed and reported in Figure 6A). TNNP04 response to changes in frequency more closely resembles experimental results, however, the model falls short in certain aspects (e.g., post rest behavior, repolarization failure when SERCA is inhibited). In our model the increased Ca transient amplitude (Figure 6A) at faster pacing rates is due to increased SR Ca load, causing larger release events and thus larger Ca transients. A small contribution is also due to $[Na]_i$ accumulation at higher frequencies, which increases the reverse mode $I_{NaCa}$ which flows for a short time early in the AP and leads to greater Ca influx during systole. Some controversy exists as to whether NCX works in forward or reverse mode during the AP plateau. Weber et al. [13] have provided direct evidence in nonfailing human myocytes (using AP clamp) that NCX extrudes Ca for most of the AP (although in failing human myocytes Ca influx via NCX was prominent during the plateau). Accordingly, $I_{NaCa}$ is normally inward over most of the plateau phase in our model (unlike previous human myocyte models). In failing myocytes, reduced subsarcolemmal Ca, increased Na, and prolonged AP may contribute to a substantial outward current during the plateau [13].

### Effects of K current block

A profound difference has been reported in the effects of $I_{Ks}$ and $I_{Kr}$ blockers on human ventricular APs. Iost et al. [19] did not detect $I_{Ks}$ in human ventricle at 35°C. Subsequently the same group [18,36] has shown that the $I_{Ks}$ blockers chromanol 293B and HMR do not significantly *lengthen* APD (<3.2%) over a broad range of pacing cycle lengths (300-5,000 ms). Our model predicts ~1 and 2.7% *prolongation* of APD at 1 and 0.2-Hz pacing rates respectively. The effect of blocking $I_{Ks}$ is quite different in other human ventricular cell models. At 1 Hz, blocking $I_{Ks}$ lengthened APD in *TNNP04 and TP06* greatly (*+38% and 74%*) [10] and mildly in *IMW* (*+8%*) [11], as reviewed in [9]. Thus, *TNNP04 and TP06* seem to overestimate the contribution of $I_{Ks}$ to basal AP repolarization, whereas in *IMW* its importance more closely resembles experiments and our model. In fact, $I_{Ks}$ has nearly the same density as in *IMW* and our model, whereas in the ten Tusscher models [8,10] $I_{Ks}$ density was set higher to reproduce results from Bosch et al. [47] showing 35% prolongation upon chromanol 293B administration in left ventricular midmyocardial cells from one patient with dilated cardiomyopathy.

At 1 Hz, Li et al. [48] reported an APD prolongation of 26% upon full $I_{Kr}$ block with E-4031, whereas Jost et al. reported an APD prolongation of ~40 and 70 ms when $I_{Kr}$ is blocked either with sotalol or E-4031 [36] and 56% prolongation with dofetilide [18]. $I_{Kr}$ current block leads to ~17% APD prolongation in the ten Tusscher models and ~31% in IMW (paced at 1 Hz). The results from the ten Tusscher and Iyer models thus are in the lower range of the experimental results, as are our model predictions (19% shortening in epicardial and 27% in endocardial myocytes).

Most importantly, in the paper by Jost et al. [36] it is shown that over the entire range of frequencies explored, d-sotalol and E-4041 markedly lengthened the AP in a reverse frequency-dependent manner [36] (Figure 7C and D). This behavior is reproduced by both our endocardial and epicardial cell models, but not by the other existing human ventricular cell models. Indeed,

in TNNP04, TP06 and IMW models increased pacing frequency caused greater predicted AP prolongation upon $I_{Kr}$ block (direct rate-dependence) (Figure S7).

Reverse rate-dependence of $I_{Kr}$ block was first explained by an increase in $I_{Ks}$ during rapid heart rates in guinea pig myocytes [49]. $I_{Ks}$ accumulation was due to the relatively slow kinetics of this current, which does not permit complete deactivation during short diastolic intervals. However, deactivation kinetics of $I_{Ks}$ in guinea pig myocytes are very slow (deactivation $\tau$~756 ms) compared to those of dog ($\tau$ ~89 ms), rabbit ($\tau$ ~157 ms) and human ($\tau$~122 ms) (all at −40 mV) [50]. Thus, the role of $I_{Ks}$ in reverse rate-dependence does not necessarily apply to species with rapid $I_{Ks}$ deactivation kinetics, where little $I_{Ks}$ accumulation occurs at physiological rapid rates (as shown by our simulations). Even when incorporating a Markov $I_{Ks}$ model [38], which predicts increases of the instantaneous and time-dependent component of $I_{Ks}$ at fast rates [39] (Figure S4), the smaller $I_{Ks}$ density compared to guinea pig makes this explanation unsatisfactory for human myocytes. In fact, reverse rate-dependence is still predicted by our model when $I_{Kr}$ is silenced in the presence of $I_{Ks}$ blockade (not shown).

We have further explored this mechanism. Figure S8 shows simulated $I_{Kr}$ traces obtained by pacing the cell at 0.5 and 2 Hz. Despite the initial spikelike increase (only at fast rates), the current peak amplitude does not change appreciably with frequency (~7% larger at 0.5 vs. 2 Hz). Accordingly, experiments from guinea pig [39], dog and human myocytes [51] did not reveal rate-dependent changes in peak $I_{Kr}$. If anything, the changes suggest that $I_{Kr}$ becomes more important at high frequency, and do not explain the reverse rate-dependence. Our results are not completely $I_{Kr}$ model-independent, since when we use the ten Tusscher formulation of the current (with our conductance value) in our comprehensive AP description, the reverse-rate dependency is maintained, but reduced. An explanation for the reverse rate-dependence was recently suggested by Zaza [52] who stated that when the AP repolarization is slower (meaning smaller net repolarizing current) a larger APD change would be expected from any change in the total membrane current. As a proof of concept, we have taken the same approach and simulated the injection of a constant inward current $I_i$ = -0.05 A/F. The effect of this *small inward* current on APD is remarkably larger when pacing the cell at low frequency (Figure S9, A) vs. fast pacing rate (Figure S9, B). To avoid any rate-dependent effect we simulated APs with different durations by clamping $[Na]_i$ at low (Figure S9, C) vs. high (Figure S9, D) levels. Similarly, APD prolongation is more marked *for* the longer initial AP, supporting the view that the same inward $I_i$ may prolong long APs more than short APs.

In human ventricular muscle selective inhibition of $I_{K1}$ with 10 μM $BaCl_2$ elicited only marginal AP prolongation (~5%), which is slightly overestimated by our model, where AP prolongs by about 10% upon 50% $I_{K1}$ block. At 1-Hz pacing rate, *TNNP04 and TP06* predict ~9% and *4%* AP prolongation *respectively*, whereas a much stronger AP prolongation (~90%) is predicted by *IMW*. Interestingly, when assessing the contribution of $I_{K1}$ to repolarization reserve (by comparing the APD change due to $I_{Kr}$ block alone and combined $I_{K1}$+$I_{Kr}$ suppression) we obtained a 30% increase in the APD attributable to the loss of $I_{K1}$ contribution, which is comparable to recent experimental observations [18]. Similarly, we estimated a lesser contribution of $I_{Ks}$ to repolarization reserve *with $I_{Kr}$ block* (22%), slightly higher than the experimental estimate (16%) [18].

We conclude that our new human ventricular myocyte model is a significant advance over previously existing models and provides a useful framework to explore ECC mechanisms and repolarization abnormalities at the single cell level. Due to its low computational cost the model may be integrated into multi-scale models of tissue and/or heart.

## Supplementary Material

Refer to Web version on PubMed Central for supplementary material.

## Acknowledgments

We thank Drs. András Varró and Norbert Jost for providing us with recent data, Drs. Stefano Severi, Antonio Zaza, Eckard Picht and Kenneth Ginsburg for valuable comments. Supported by *NIH* R37-HL30077, P01-HL80101, a grant from the Fondation Leducq (to D.M.B) and the Max Schaldach Fellowship in Cardiac Pacing and Electrophysiology from the Heart Rhythm Society (to E.G.).

## References

1. Faber GM, Rudy Y. Action Potential and Contractility Changes in $[Na^+]_i$ Overloaded Cardiac Myocytes: A Simulation Study. Biophys J 2000;78(5):2392. [PubMed: 10777735]
2. Shannon TR, Wang F, Puglisi J, Weber C, Bers DM. A Mathematical Treatment of Integrated Ca Dynamics within the Ventricular Myocyte. Biophys J 2004;87(5):3351. [PubMed: 15347581]
3. Bondarenko VE, Szigeti GP, Bett GCL, Kim SJ, Rasmusson RL. Computer model of action potential of mouse ventricular myocytes. Am J Physiol Heart Circ Physiol 2004;287(3):H1378–1403. [PubMed: 15142845]
4. Hund TJ, Rudy Y. Rate Dependence and Regulation of Action Potential and Calcium Transient in a Canine Cardiac Ventricular Cell Model. Circulation 2004;110(20):3168–3174. [PubMed: 15505083]
5. Grandi E, Puglisi JL, Wagner S, Maier LS, Severi S, Bers DM. Simulation of Ca-Calmodulin-Dependent Protein Kinase II on Rabbit Ventricular Myocyte Ion Currents and Action Potentials. Biophys J 2007;93(11):3835. [PubMed: 17704163]
6. Clancy CE, Zhu ZI, Rudy Y. Pharmacogenetics and anti-arrhythmic drug therapy: a theoretical investigation. Am J Physiol Heart Circ Physiol 2007;292(1):H66–75. [PubMed: 16997895]
7. Priebe L, Beuckelmann DJ. Simulation Study of Cellular Electric Properties in Heart Failure. Circ Res 1998;82(11):1206–1223. [PubMed: 9633920]
8. ten Tusscher KHWJ, Panfilov AV. Alternans and spiral breakup in a human ventricular tissue model. Am J Physiol Heart Circ Physiol 2006;291(3):H1088–1100. [PubMed: 16565318]
9. ten Tusscher KHWJ, Panfilov AV. Cell model for efficient simulation of wave propagation in human ventricular tissue under normal and pathological conditions. Physics in Medicine and Biology 2006;51 (23):6141. [PubMed: 17110776]
10. ten Tusscher KHWJ, Noble D, Noble PJ, Panfilov AV. A model for human ventricular tissue. Am J Physiol Heart Circ Physiol 2004;286(4):H1573–1589. [PubMed: 14656705]
11. Iyer V, Mazhari R, Winslow RL. A Computational Model of the Human Left-Ventricular Epicardial Myocyte. Biophys J 2004;87(3):1507–1525. [PubMed: 15345532]
12. Bernus O, Wilders R, Zemlin CW, Verschelde H, Panfilov AV. A computationally efficient electrophysiological model of human ventricular cells. Am J Physiol Heart Circ Physiol 2002;282 (6):H2296–2308. [PubMed: 12003840]
13. Weber CR, Piacentino V III, Houser SR, Bers DM. Dynamic Regulation of Sodium/Calcium Exchange Function in Human Heart Failure. Circulation 2003;108(18):2224–2229. [PubMed: 14557358]
14. Virág L, Iost N, Opincariu M, Szolnoky J, Szécsi J, Bogats G, Szenohradszky P, Varró A, Papp JG. The slow component of the delayed rectifier potassium current in undiseased human ventricular myocytes. Cardiovasc Res 2001;49(4):790–797. [PubMed: 11230978]
15. Zhou Z, Gong Q, Ye B, Fan Z, Makielski JC, Robertson GA, January CT. Properties of HERG channels stably expressed in HEK 293 cells studied at physiological temperature. Biophys J 1998;74 (1):230–241. [PubMed: 9449325]
16. Johnson JP Jr, Mullins FM, Bennett PB. Human Ether-a-go-go-related Gene $K^+$ Channel Gating Probed with Extracellular $Ca^{2+}$. Evidence for Two Distinct Voltage Sensors. J Gen Physiol 1999;113 (4):565–580. [PubMed: 10102937]

17. Jost N, Varró A, Szüts V, Kovács PP, Seprényi G, Biliczki P, Lengyel C, Prorok J, Bitay M, Ördög B, Szabad J, Varga-Orvos Z, Puskás LG, Cotella D, Papp JG, Virág L, Nattel S. Molecular basis of repolarization reserve differences between dogs and man. Circulation 2008;118(8):S342. abstract.
18. Jost N, Virág L, Szüts V, Seprényi G, Biliczki P, Lengyel C, Bitay M, Ördög B, Koncz I, Nagy N, Kovács M, Szabad J, Varga-Orvos Z, Puskás LG, Cotella D, Wettwer E, Ravens U, Papp JG, Varró A, Nattel S. Weaker inward-rectifier ($I_{K1}$) and slow delayed-rectifier ($I_{Ks}$) potassium currents limit cardiac repolarization reserve in humans compared to dogs. Circ Res. 2009 in press.
19. Iost N, Virág L, Opincariu M, Szécsi J, Varró A, Papp JG. Delayed rectifier potassium current in undiseased human ventricular myocytes. Cardiovasc Res 1998;40(3):508–515. [PubMed: 10070491]
20. Magyar J, Iost N, Körtvély Á, Bányász T, Virág L, Szigligeti P, Varró A, Opincariu M, Szécsi J, Papp JG, Nánási PP. Effects of endothelin-1 on calcium and potassium currents in undiseased human ventricular myocytes. Pflügers Archiv European Journal of Physiology 2000;441(1):144.
21. Näbauer M, Beuckelmann DJ, Uberfuhr P, Steinbeck G. Regional Differences in Current Density and Rate-Dependent Properties of the Transient Outward Current in Subepicardial and Subendocardial Myocytes of Human Left Ventricle. Circulation 1996;93(1):168–177. [PubMed: 8616924]
22. Wettwer E, Amos J, Posival H, Ravens U. Transient outward current in human ventricular myocytes of subepicardial and subendocardial origin. Circ Res 1994;75(3):473–482. [PubMed: 8062421]
23. Varró A, Virág L, Acsai K, Jost N, Lengyel C, Papp JG. Role of the slowly inactivating transient outward potassium current in cardiac repolarization. Heart Rhythm 2006;3(5):S302. abstract.
24. Shampine LF, Reichelt MW. The MATLAB ODE Suite. SIAM Journal on Scientific Computing 1997;18:1–22.
25. Morgan JM, Cunningham D, Rowland E. Electrical restitution in the endocardium of the intact human right ventricle. Br Heart J 1992;67(1):42–46. [PubMed: 1739524]
26. Drouin E, Lande G, Charpentier F. Amiodarone reduces transmural heterogeneity of repolarization in the human heart. J Am Coll Cardiol 1998;32(4):1063–1067. [PubMed: 9768733]
27. Li GR, Feng J, Yue L, Carrier M. Transmural heterogeneity of action potentials and Ito1 in myocytes isolated from the human right ventricle. Am J Physiol Heart Circ Physiol 1998;275(2):H369–377.
28. Piacentino V III, Weber CR, Chen X, Weisser-Thomas J, Margulies KB, Bers DM, Houser SR. Cellular Basis of Abnormal Calcium Transients of Failing Human Ventricular Myocytes. Circ Res 2003;92(6):651–658. [PubMed: 12600875]
29. Li GR, Yang B, Feng J, Bosch RF, Carrier M, Nattel S. Transmembrane $I_{Ca}$ contributes to rate-dependent changes of action potentials in human ventricular myocytes. Am J Physiol Heart Circ Physiol 1999;276(1):H98–106.
30. Pereon Y, Demolombe S, Baro I, Drouin E, Charpentier F, Escande D. Differential expression of KvLQT1 isoforms across the human ventricular wall. Am J Physiol Heart Circ Physiol 2000;278(6):H1908–1915. [PubMed: 10843888]
31. Weber CR, Piacentino V III, Ginsburg KS, Houser SR, Bers DM. $Na^+$-$Ca^{2+}$ Exchange Current and Submembrane [$Ca^{2+}$] During the Cardiac Action Potential. Circ Res 2002;90(2):182–189. [PubMed: 11834711]
32. Pieske B, Kretschmann B, Meyer M, Holubarsch C, Weirich J, Posival H, Minami K, Just H, Hasenfuss G. Alterations in Intracellular Calcium Handling Associated With the Inverse Force-Frequency Relation in Human Dilated Cardiomyopathy. Circulation 1995;92(5):1169–1178. [PubMed: 7648662]
33. Li GR, Lau CP, Leung TK, Nattel S. Ionic current abnormalities associated with prolonged action potentials in cardiomyocytes from diseased human right ventricles. Heart Rhythm 2004;1(4):460. [PubMed: 15851200]
34. Schmidt U, Hajjar RJ, Helm PA, Kim CS, Doye AA, Gwathmey JK. Contribution of Abnormal Sarcoplasmic Reticulum ATPase Activity to Systolic and Diastolic Dysfunction in Human Heart Failure. J Mol Cell Cardiol 1998;30(10):1929. [PubMed: 9799647]
35. Pieske B, Maier LS, Piacentino V III, Weisser J, Hasenfuss G, Houser S. Rate Dependence of [$Na^+$]$_i$ and Contractility in Nonfailing and Failing Human Myocardium. Circulation 2002;106(4):447–453. [PubMed: 12135944]

36. Jost N, Virág L, Bitay M, Takács J, Lengyel C, Biliczki P, Nagy Z, Bogats G, Lathrop DA, Papp JG, Varró A. Restricting Excessive Cardiac Action Potential and QT Prolongation: A Vital Role for $I_{Ks}$ in Human Ventricular Muscle. Circulation 2005;112(10):1392–1399. [PubMed: 16129791]
37. Varró A, Baláti B, Iost N, Takács J, Virág L, Lathrop D, Csaba L, Tálosi L, Papp J. The role of the delayed rectifier component $I_{Ks}$ in dog ventricular muscle and Purkinje fibre repolarization. J Physiol 2000;523(Pt 1):67–81. [PubMed: 10675203]
38. Silva J, Rudy Y. Subunit Interaction Determines $I_{Ks}$ Participation in Cardiac Repolarization and Repolarization Reserve. Circulation 2005;112(10):1384–1391. [PubMed: 16129795]
39. Rocchetti M, Besana A, Gurrola G, Possani L, Z A. Rate dependency of delayed rectifier currents during the guinea-pig ventricular action potential. J Physiol 2001;534(Pt 3):721–732. [PubMed: 11483703]
40. Xiong W, Tian Y, DiSilvestre D, Tomaselli GF. Transmural heterogeneity of $Na^+$-$Ca^{2+}$ exchange: evidence for differential expression in normal and failing hearts. Circ Res 2005;97(3):207–209. [PubMed: 16002750]
41. Laurita KR, K R, Wible B, Wan X, Koo MH. Transmural heterogeneity of calcium handling in canine. Circ Res 2003;92(6):668–675. [PubMed: 12600876]
42. Prestle J, Dieterich S, Preuss M, Bieligk U, Hasenfuss G. Heterogeneous transmural gene expression of calcium-handling proteins and natriuretic peptides in the failing human heart. Cardiovasc Res 1999;43(2):323–331. [PubMed: 10536662]
43. Gao J, Wang W, Cohen IS, Mathias RT. Transmural Gradients in Na/K Pump Activity and $[Na^+]_i$ in Canine Ventricle. 2005;89(3):1700.
44. Weisser-Thomas J, Piacentino V III, Gaughan JP, Margulies K, Houser SR. Calcium entry via Na/Ca exchange during the action potential directly contributes to contraction of failing human ventricular myocytes. Cardiovasc Res 2003;57(4):974–985. [PubMed: 12650875]
45. Rocchetti M, Besana A, Mostacciuolo G, Ferrari P, Micheletti R, Zaza A. Diverse Toxicity Associated with Cardiac $Na^+/K^+$ Pump Inhibition: Evaluation of Electrophysiological Mechanisms. J Pharmacol Exp Ther 2003;305(2):765–771. [PubMed: 12606646]
46. Hordof AJ, Spotnitz A, Mary-Rabine L, Edie RN, Rosen MR. The cellular electrophysiologic effects of digitalis on human atrial fibers. Circulation 1978;57(2):223–229. [PubMed: 618608]
47. Bosch RF, Gaspo R, Busch AE, Lang HJ, Li GR, Nattel S. Effects of the chromanol 293B, a selective blocker of the slow, component of the delayed rectifier $K^+$ current, on repolarization in human and guinea pig ventricular myocytes. Cardiovasc Res 1998;38(2):441–450. [PubMed: 9709405]
48. Li GR, Feng J, Yue L, Carrier M, Nattel S. Evidence for Two Components of Delayed Rectifier $K^+$ Current in Human Ventricular Myocytes. Circ Res 1996;78(4):689–696. [PubMed: 8635226]
49. Jurkiewicz NK, Sanguinetti MC. Rate-dependent prolongation of cardiac action potentials by a methanesulfonanilide class III antiarrhythmic agent. Specific block of rapidly activating delayed rectifier $K^+$ current by dofetilide. Circ Res 1993;72(1):75–83. [PubMed: 8417848]
50. Jost N, Papp JG, Varró A. Slow Delayed Rectifier Potassium Current ($I_{Ks}$) and the Repolarization Reserve. Annals of Noninvasive Electrocardiology 2007;12(1):64–78. [PubMed: 17286653]
51. Virág L, Acsai K, Hála O, Zaza A, Bitay M, Bogáts G, Papp JG, Varró A. Self-augmentation of the lengthening of repolarization is related to the shape of the cardiac action potential: implications for reverse rate dependency. Br J Pharmacol 2009;156(7):1076–1084. [PubMed: 19226285]
52. Zaza A. Control of the cardiac action potential: the role of repolarization dynamics. J Mol Cell Cardiol. in press.


## Abbreviations

| | |
|---|---|
| AP | Action Potential |
| APD | Action Potential Duration |
| ECC | Excitation-Contraction Coupling |
| SL | Subsarcolemma |
| SR | Sarcoplasmic Reticulum |

| | |
|---|---|
| SERCA | SR Ca-ATPase |
| NXC | Na-Ca exchanger |
| TNNP04 | ten Tusscher-Noble-Noble-Panfilov model |
| TP06 | ten Tusscher-Panfilov model |
| IMW | Iyer-Mazhari-Winslow model |

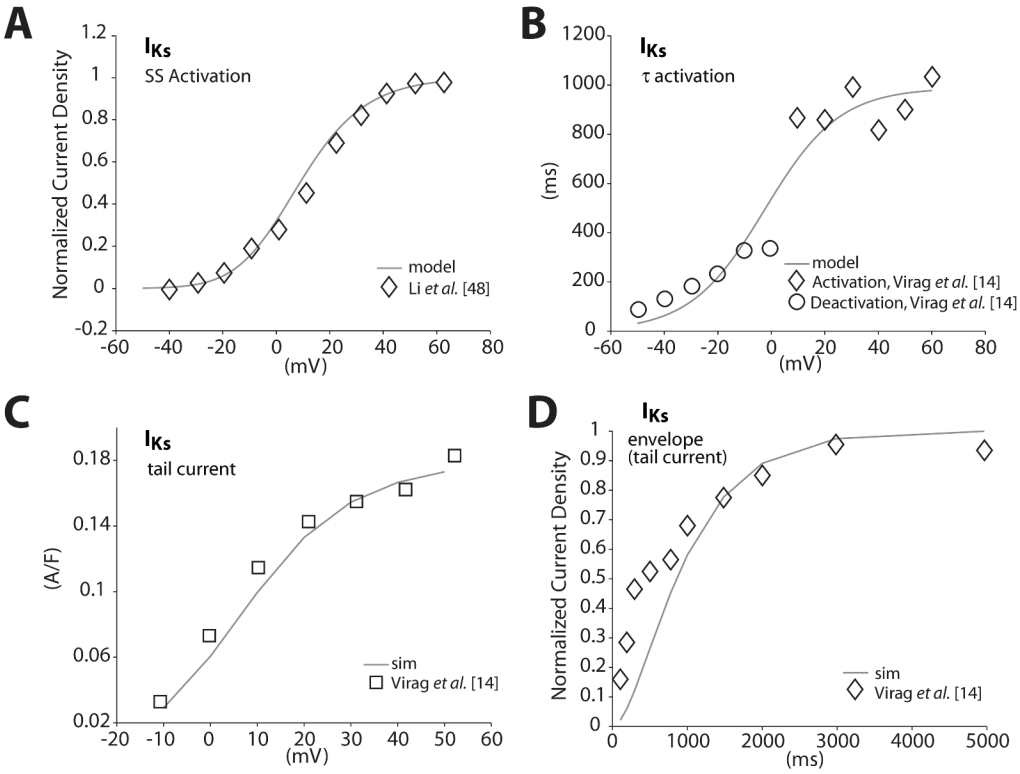


**Figure 1.**

Gating properties of $I_{Ks}$. Model curves (*lines*) and data (*symbols*) from Li et al. [48] and Virág et al. [14] are shown. *A*: Steady-state activation. *B*: Activation and deactivation time constants. *C*: Current-voltage relationship. Tail $I_{Ks}$ was measured during 5,000-ms voltage steps to potentials shown from a holding potential of −40 mV. *D*: Envelope test protocol assessing the kinetics of $I_{Ks}$ activation.

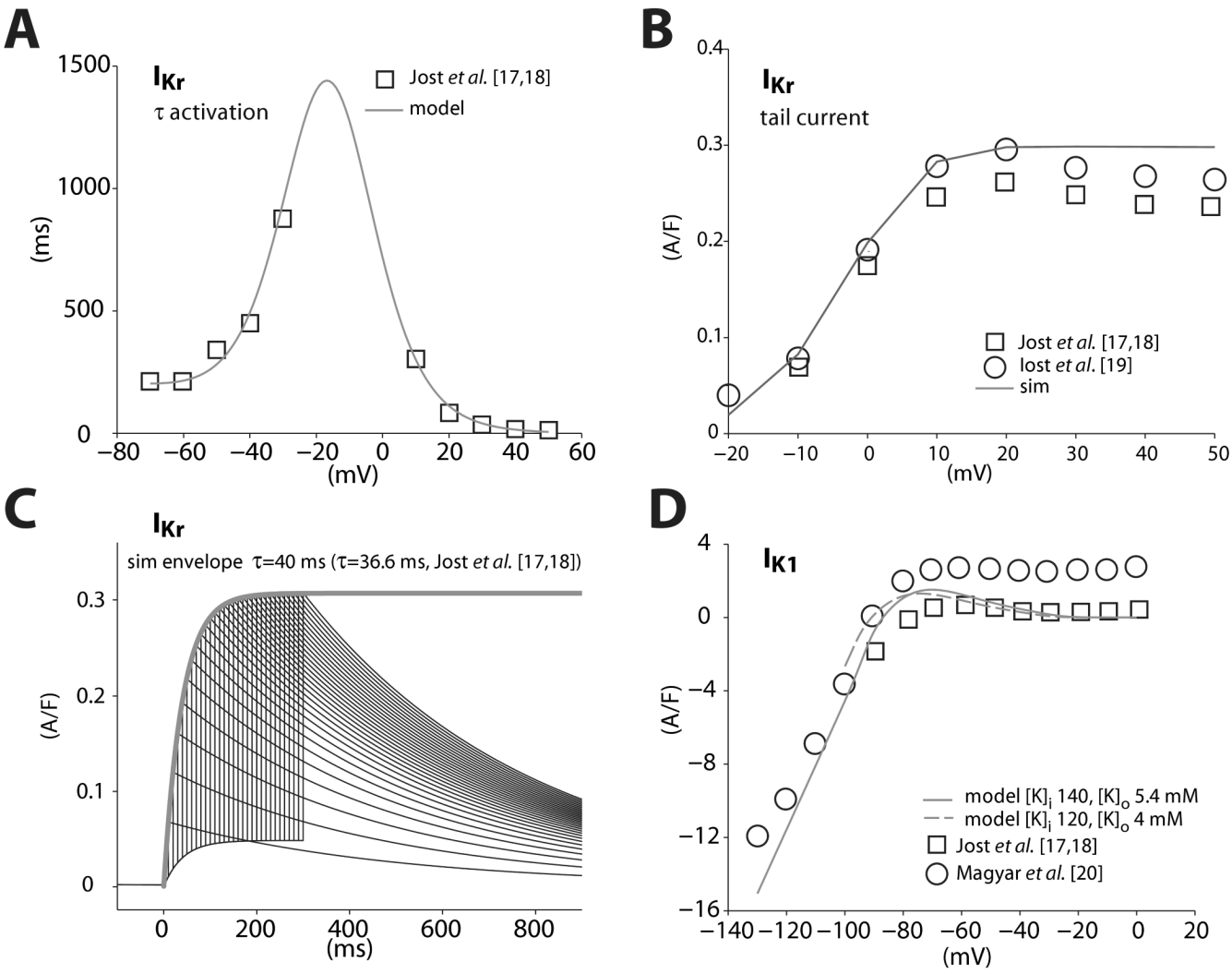


**Figure 2.**

Gating properties of $I_{Kr}$ and $I_{K1}$. Model curves (*lines*) and data (*symbols*) from Jost et al. [17, 18], Iost et al. [19] and Magyar et al. [20] are shown. *A*: Activation and deactivation time constants. *B:* $I_{Kr}$ current-voltage relationship. Tail $I_{Kr}$ was measured during 1,000-ms voltage steps to potentials shown from a holding potential of −40 mV. *C*: Simulated envelope test protocol assessing $I_{Kr}$ activation time constant at +30 mV. *D*: Steady-state current-voltage relationships of $I_{K1}$.

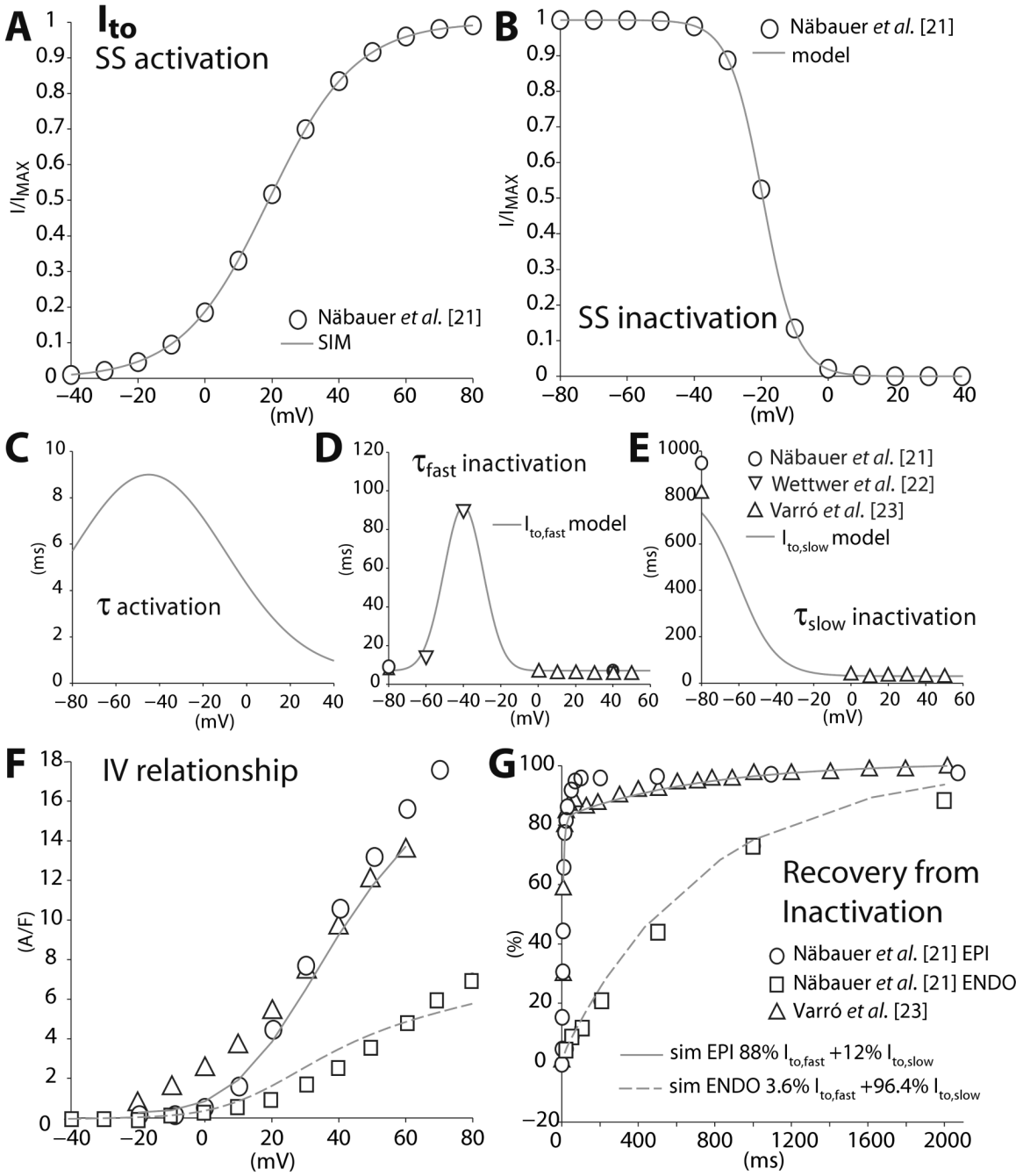


**Figure 3.**

Gating properties of $I_{to}$. Model curves (*lines*) and data (*symbols*) from Näbauer et al. [21], Wettwer et al. [22] and Varró et al. [23] are shown. *A*: Steady-state activation. *B*: Steady-state inactivation. *C*: Activation time constants of $I_{to,fast}$ and $I_{to,slow}$ are unchanged from Shannon et al. [2]. *D*: Inactivation time constants of $I_{to,fast}$ and *E:* $I_{to,slow}$. *F*: Epicardial and endocardial $I_{to}$ current-voltage curves. *G*: Recovery from inactivation of epicardial and endocardial $I_{to}$ was assessed with a two pulse (500 ms from −80 to 50 mV) protocol with varying interpulse intervals.

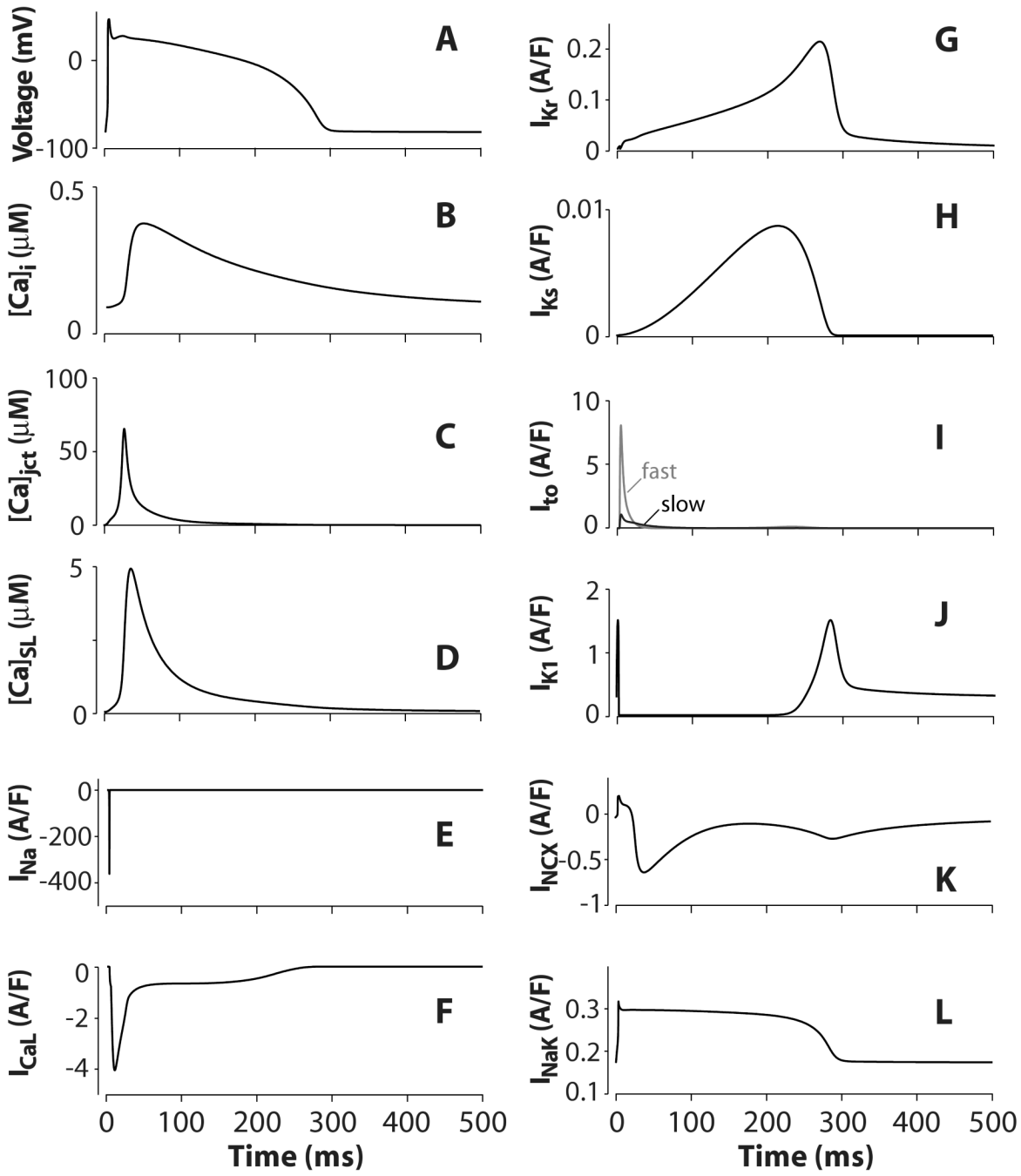


**Figure 4.**

Steady-state epicardial AP, calcium transient, and major ionic currents simulated at 1-Hz pacing rate. *A*: Action potential. *B*: Cytosolic [Ca]. *C*: Junctional [Ca]. *D*: SL [Ca]. *E*: Fast sodium current. *F*: L-type calcium current. G: Rapidly activating delayed rectifier potassium current. *H*: Slowly activating delayed rectifier potassium current. *I*: Slowly and rapidly inactivating transient outward potassium currents. *J*: Inward rectifier potassium current. *K*: Sodium-calcium exchange current. *L*: Sodium-potassium ATPase current.

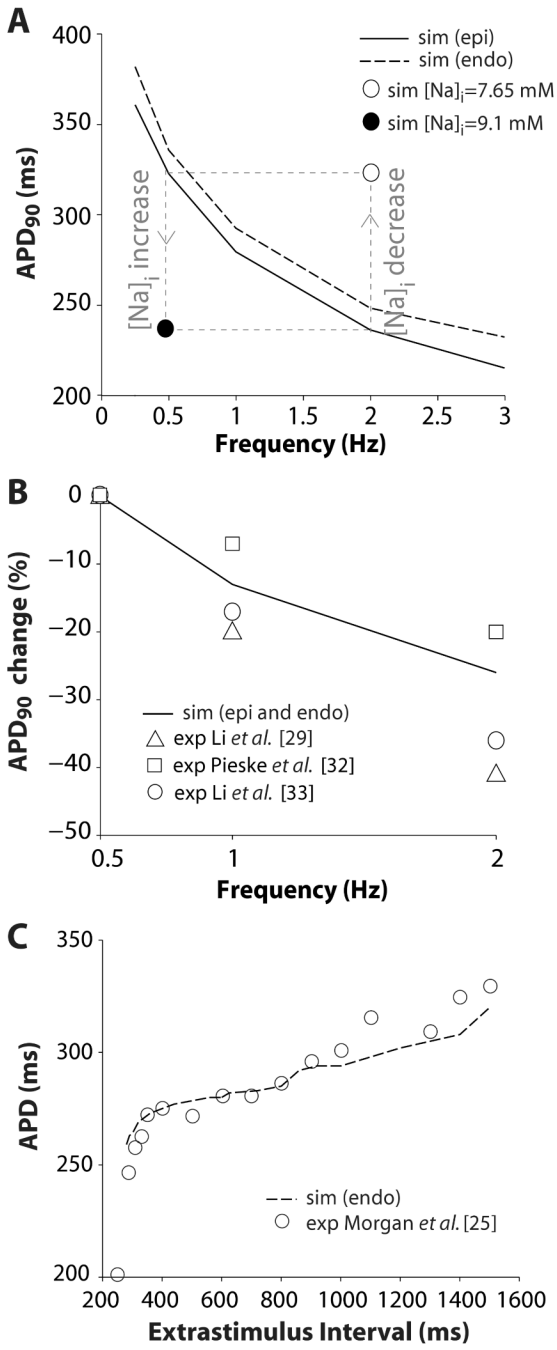


**Figure 5.**

*A*: Simulated APD adaptation curves. Steady-state APD of human epicardial (solid line) and endocardial (dashed line) ventricular cell models shortened as pacing rate was made faster. *B*: Fractional $APD_{90}$ changes on increasing pacing frequency from 0.5 to 1 and 2 Hz. Simulated results (solid line) are within the range of experimental variability (data are from references [29,32,33], symbols). *C*: Simulated endocardial APD restitution curve (dashed line), compared with experimental data (circles) from endocardial monophasic APs in human hearts [25].

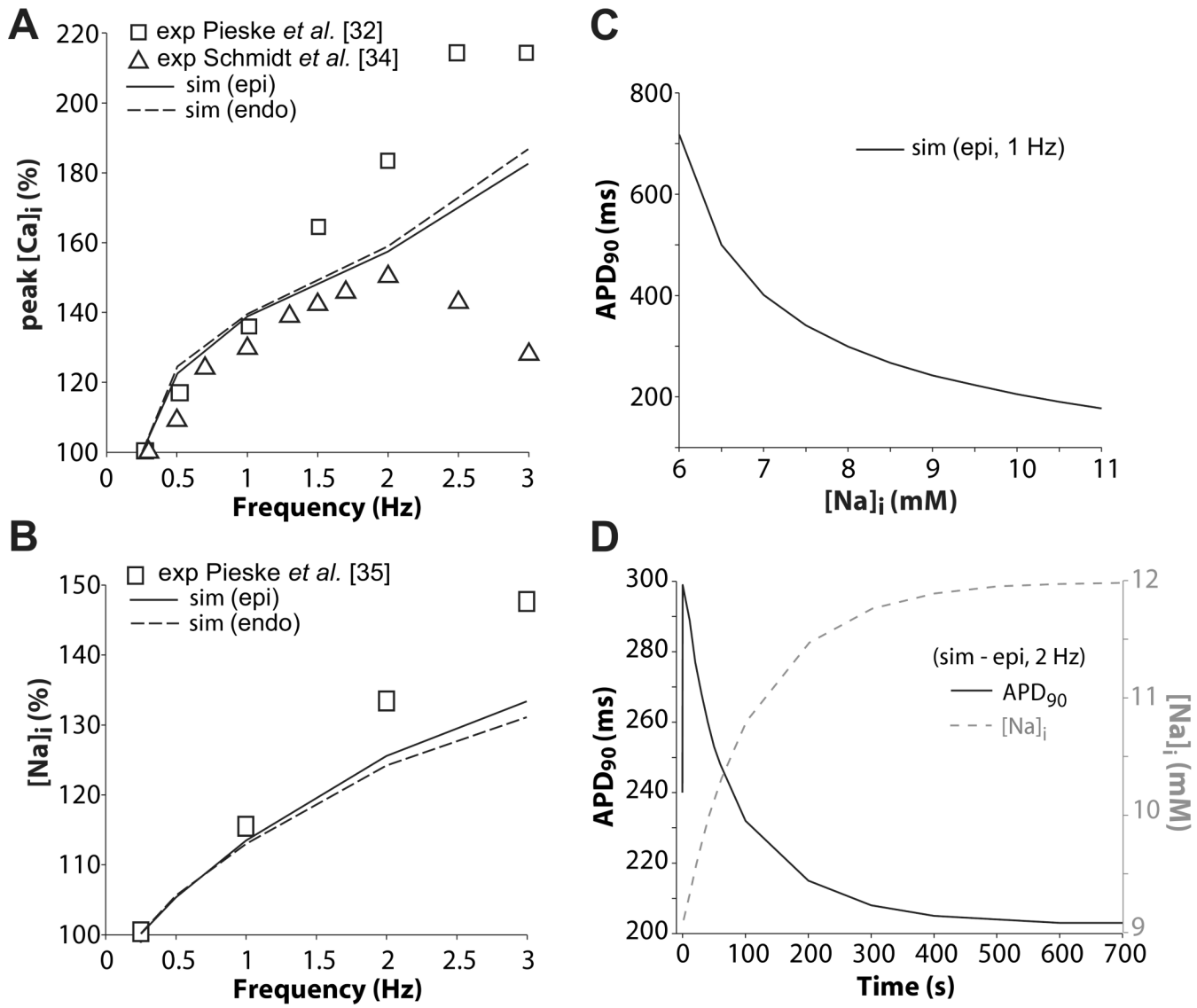


**Figure 6.**

*A*: Fractional changes in peak $[Ca]_i$ and *B*: $[Na]_i$ at increasing pacing frequencies in the human epicardial (solid lines) and endocardial (dashed lines) ventricular myocyte models. Experimental results (symbols) are from references [32,34] and [35]. *C*: Predicted $APD_{90}$ dependency on $[Na]_i$ (epicardium, 1 Hz). *D*: Simulated Na pump blockade (50%) caused AP prolongation followed by gradual shortening as Na ions accumulated in the cytosol (epicardium, 2 Hz).

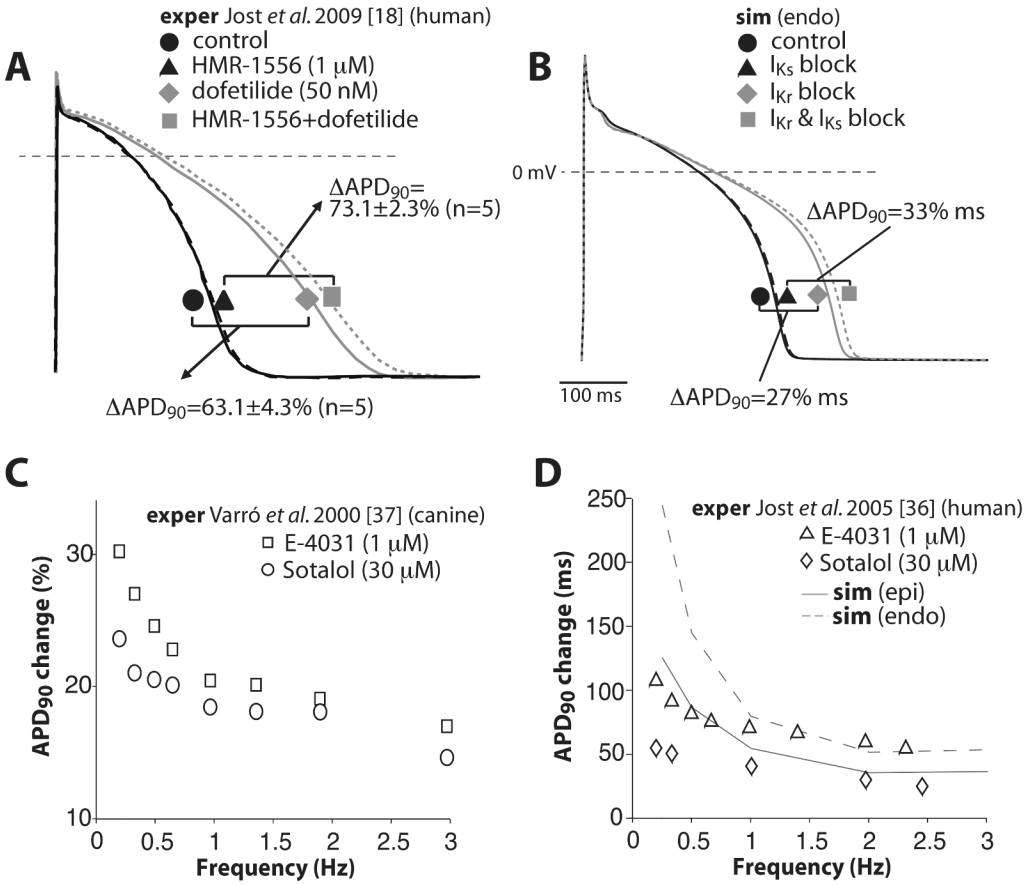


**Figure 7.**

Contribution of $I_{Ks}$ and $I_{Kr}$ to ventricular repolarization and repolarization reserve. *A*: Effects of $I_{Ks}$ (HMR-1556), $I_{Kr}$ (dofetilide), and combined ($I_{Ks}$+$I_{Kr}$) block on APD in isolated human myocytes. Redrawn from [18]. *B*: Simulations predicted a large effect of $I_{Kr}$ block on APD, no effect of $I_{Ks}$ on basal APD and modest contribution to repolarization reserve. *C, D:* $I_{Kr}$ blockers prolonged APD in a reverse-frequency-dependent manner. Model predictions (*D*, lines) agree with experimental findings (symbols) in (*C*) canine [37] and (*D*) human ventricular myocytes [36].

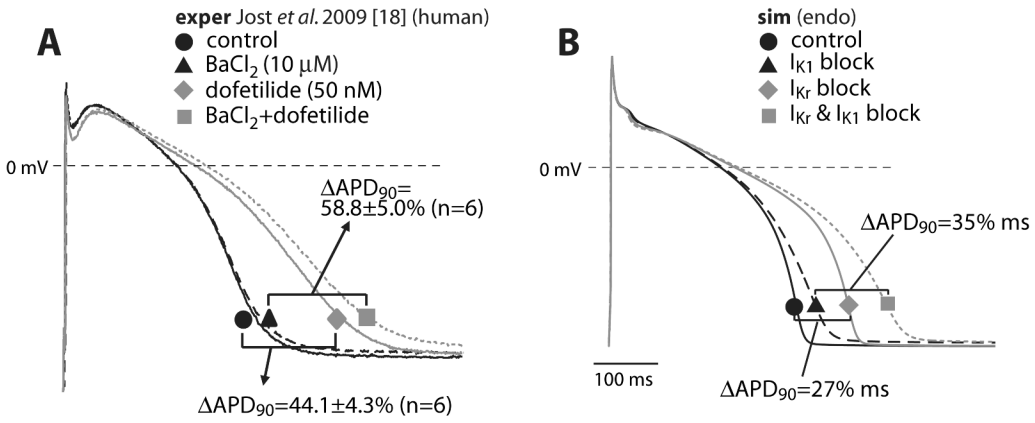


**Figure 8.**

Contribution of $I_{K1}$ to ventricular repolarization and repolarization reserve. *A*: Effect of $I_{K1}$ ($BaCl_2$), $I_{Kr}$ (dofetilide) and combined ($I_{K1}$+$I_{Kr}$) block on APD in isolated human myocytes. Redrawn from [18]. *B*: Simulated results predict a modest AP prolongation upon $I_{K1}$ block and a more significant contribution of $I_{K1}$ to repolarization reserve.